Two-dimensional nano-sheets produced by liquid exfoliation of layered materials

Jonathan N Coleman[1*], Mustafa Lotya[1], Arlene O'Neill[1], Shane D Bergin[1], Paul J King[1], Umar Khan[1], Karen Young[1], Alexandre Gaucher[1], Sukanta De[1], Ronan J Smith,[1] Igor V Shvets[1], Sunil K Arora[1], George Stanton[1], Hye-Young Kim[2,3], Kangho Lee[2,3], Gyu Tae Kim[3], Georg S Duesberg[2], Toby Hallam[2], John J Boland[2], Jing Jing Wang,[1] John F Donegan,[1] Jaime C Grunlan[4], Gregory Moriarty[4], Aleksey Shmeliov[5], Rebecca J Nicholls[5], James M Perkins[6], Eleanor M. Grieveson[5], Koenraad Theuwissen[5], David W. McComb[6], Peter D. Nellist[5] and Valeria Nicolosi[5*]

[1]*School of Physics and CRANN, Trinity College Dublin, D2, Ireland*

[2]*School of Chemistry and CRANN, Trinity College Dublin, D2, Ireland*

[3]*School of Electrical Engineering, Korea University, Seoul, South Korea*

[4]*Department of Mechanical Engineering, Texas A and M University, College Station, Texas 77843, USA*

[5]*Department of Materials, University of Oxford, Parks Road, Oxford OX1 3PH, UK*

[6]*Department of Materials, Imperial College London, London, SW7 2AZ, UK*

**colemaj@tcd.ie, valeria.nicolosi@materials.ox.ac.uk*

One sentence summary:

We describe a general liquid-phase method to exfoliate layered compounds to give mono- and few-layer flakes in large quantities.

Abstract

If they could be easily exfoliated, layered materials would become a diverse source of 2-dimensional crystals whose properties would be useful in applications from electronics to energy storage. We show that layered compounds such as MoS_2, WS_2, $MoSe_2$, $MoTe_2$, $TaSe_2$, $NbSe_2$, $NiTe_2$, BN and Bi_2Te_3, can be efficiently dispersed in common solvents and can be deposited as individual flakes or formed into films. Electron microscopy confirms the material to be exfoliated into individual layers. By blending with suspensions of other nano-materials or polymer solutions, we can prepare hybrid dispersions or composites which can be cast into films. We show that WS_2 and MoS_2 effectively reinforce polymers, while WS_2/carbon nanotube hybrid films have high conductivity leading to promising thermoelectric properties.

Layered materials represent a diverse and largely untapped source of 2-dimensional (2D) systems with exotic electronic properties and high specific surface areas that are important for sensing, catalysis and energy storage applications. While graphene is the most well-known layered material, transition metal dichalcogenides (TMDs), transition metal oxides (TMOs) and other 2D compounds such as BN, Bi_2Te_3 and Bi_2Se_3 are also important. The latter materials are of particular interest as topological insulators and thermoelectric materials(*1*). However, development of these materials has been hampered by the lack of a simple method to exfoliate them to give mono- or few-layer flakes in large quantities.

TMDs consist of hexagonal layers of metal atoms, M, sandwiched between two layers of chalcogen atoms, X, with stoichiometry MX_2. While the bonding within these tri-layer sheets is covalent, adjacent sheets stack via van der Waals interactions to form a 3D crystal. TMDs occur in more than 40 different types (*2, 3*) depending on the combination of chalcogen (S, Se or Te) and transition metal(*3*). Depending on the co-ordination and oxidation state of the metal atoms, TMDs can be metallic, semi-metallic or semiconducting(*2, 3*), e.g. WS_2 is a semiconductor while $NbSe_2$ is a metal(*3*). In addition, superconductivity(*4*) and charge density wave effects(*5*) have been observed in some TMDs. This versatility makes them potentially useful in many areas of electronics.

However, like graphene(*6*), layered materials must be exfoliated to fulfil their full potential. For example, films of exfoliated Bi_2Te_3 should display enhanced thermoelectric efficiency by suppression of thermal conductivity(*7*). Exfoliation of 2D topological insulators such as Bi_2Te_3 and Bi_2Se_3 would reduce residual bulk conductance,

highlighting surface effects. In addition, we can expect changes in electronic properties as the number of layers is reduced e.g. the indirect bandgap of bulk MoS_2 becomes direct in few-layer flakes(*8*). Although exfoliation can be achieved mechanically on a small scale(*9, 10*), liquid phase exfoliation methods are required for many applications(*11*). Critically, a simple liquid exfoliation method would allow the formation of novel hybrid and composite materials. While TMDs can be chemically exfoliated in liquids(*12-14*), this method is time consuming, extremely sensitive to the environment and incompatible with most solvents.

We demonstrate exfoliation of bulk TMD crystals in common solvents to give mono- and few layer nano-sheets. This method is insensitive to air and water and can potentially be scaled up to give large quantities of exfoliated material. In addition, we show that this procedure allows the formation of hybrid films with enhanced properties.

We initially sonicated commercial MoS_2, WS_2 and BN (*15, 16*) powders in a number of solvents with varying surface tensions. The resultant dispersions were centrifuged and the supernatant decanted (Section S3). Optical absorption spectroscopy showed that the amount of material retained (characterised by $A/l = \alpha C$, where A/l is the absorbance per length, α is the extinction coefficient and C is the concentration) was maximised for solvents with surface tension close to 40 mJ/m^2(*17, 18*) (Fig. 1A-C). Detailed analysis, within the framework of Hansen solubility parameter theory(*19*), shows successful solvents to be those with dispersive, polar and H-bonding components of the cohesive energy density within certain well-defined ranges (Section S4, Figs. S2-S3). This can be interpreted to mean that successful solvents are those which minimise the energy of

exfoliation. Importantly, this information will facilitate the search for new solvents and the development of solvent blends. Some of the more promising solvents were N-methyl-pyrrolidone (NMP) and isopropanol (IPA)(see Table S1 for full solvent list). Optimization of the dispersion procedure (Section S5), gave concentrations as high as 0.3 mg/ml for MoS_2, 0.15 mg/ml for WS_2 (both in NMP) and 0.06 mg/ml for BN (IPA). Photographs of typical dispersions, which are stable over periods of 100s of hours (Section S8, Fig. S13), are shown in Fig. 1D. Optical absorption spectra (Fig. 1E) show features expected for MoS_2 and WS_2(*20, 21*). In addition, a band edge at ~5 eV is clearly observed for dispersed BN. However, the spectra appear to be superimposed on a background, possibly due to scattering (Section S6, Fig. S4). A/l scaled linearly with concentration for all samples, allowing calculation of α values (Fig. 1F).

We performed TEM analysis on our dispersions, typically observing 2D flakes consisting of thin nanosheets. Examples of very thin sheets observed for all three materials are shown in Fig. 2A-C. The lateral size of these objects was typically 50-1000 nm for MoS_2 and WS_2 and 100-5000 nm for BN. (Section S7, Figs. S5-S12). We can examine these objects in more detail using aberration corrected TEM (Figs. 2D-F). These images and associated Fourier transforms illustrate the hexagonal symmetry of these materials. This is in contrast to reports on MoS_2 and WS_2 exfoliated by lithium intercalation which results in significant deviation from hexagonal structure (*22-24*). Fig. 2G-I show sections of the images in Fig. 2D-F after performing low-pass Butterworth filtering. These images reveal B-N bond lengths of 1.45Å and MoS_2 and WS_2 hexagon widths of 3.8 Å and 4 Å, confirming that no distortions have been introduced by exfoliation. Analysis of TEM

intensity profiles, coupled with flake edge analysis, electron diffraction and EELS data suggest the presence of mono-sheets in the sample(*25*).

Our dispersion/exfoliation method allowed us to prepare films of BN, MoS_2 and WS_2 by vacuum filtration(*17*) or spraying, with thickness ranging from a few nm to hundreds of microns. Photographs of free-standing films are shown in Fig. 3A. Scanning electron and helium ion microscopy of the surface and edges of these films shows them to consist of partially aligned 2D platelets (Figs. 3B,C and S17). The versatility of the solvent-exfoliation method makes it simple to create hybrid dispersions and films simply by adding another material to the dispersion. We illustrated this by preparing hybrid films of MoS_2 or WS_2 mixed with graphene or single-walled nanotubes (SWNT) (Fig. 3D, E and Section S10). With the exception of pure BN, all films were mechanically robust (Section S10, Figs. S18, S20). Addition of graphene or SWNTs increased the DC conductivity, σ_{DC}, from ~10^{-6} S/m for the TMD-only films to ~2×10^{4} S/m for the SWNT based hybrids (Fig. 3F). We performed thermoelectric measurements on free-standing WS_2/SWNT hybrid films, measuring σ_{DC} and the Seebeck coefficient, S. Obtaining significant increases in σ_{DC} without degrading S to give high power factor ($S^2\sigma_{DC}$) is critically important in thermoelectric research(*26*). Here $S^2\sigma_{DC}$ increases from 0.2 $\mu W/K^2m$ for disordered WS_2 films (*27*) to >100 $\mu W/K^2m$ for WS_2/SWNT films (Fig. 3G, Section S10).

Solvent processing greatly simplifies composite preparation (*28-31*), allowing us to prepare composites of polyurethane filled with BN, MoS_2 and WS_2. We observed

significant levels of reinforcement, comparable to the best results achieved using graphene(*32*) or nanoclays(*33*) as fillers (Figs. 3H, S19 and S20).

Exfoliated flakes can be deposited on substrates by spraying. Shown in Fig. 4A and B are an SEM and an AFM image of a silicon wafer spraycoated with MoS_2. The objects observed are hundreds of nm wide in agreement with the TEM data (*25*). We can confirm the flakes consist of MoS_2 by Raman mapping (Fig. 4C), based on the individual flake spectrum shown in Fig. 4D. We note that the peak positions(*25, 34*) in Fig. 4D are consistent with trigonal prismatic (2H) mono- or bi-layer MoS_2 (Section S9). SEM analysis (Fig. 4 E-H) shows that while some deposited flakes are very thin, many are multilayers or clusters which have aggregated during deposition. AFM and STM imaging of individual flakes shows them to display typical thicknesses of ~3-12 nm (Figs. 4 H-J, S15, S16, Section S9). Some of these images, particularly the STM image in Fig. 4L, show steps. These are consistently ~1nm high and probably originate in layer edges. Electrical characterisation of individual flakes shows n-type field-effect behaviour characterised by mobilities of ~0.01 cm^2/Vs (*9, 10*), rather lower than observed for mechanically exfoliated MoS_2 flakes (Section S11).

This exfoliation process is not limited to BN, MoS_2 and WS_2. We have exfoliated $MoSe_2$, $MoTe_2$, $TaSe_2$, $NbSe_2$, $NiTe_2$ and Bi_2Te_3 in a number of the solvents in table S1 (Section S12, Figs. S23, S24), and believe similar solvents may exfoliate all MX_2 compounds. We propose that this exfoliation technique is general as it can be applied to TMDs, graphene, BN and Bi_2Te_3. As such, we expect to extend it to TMOs(*35*) and other layered compounds.

Figs

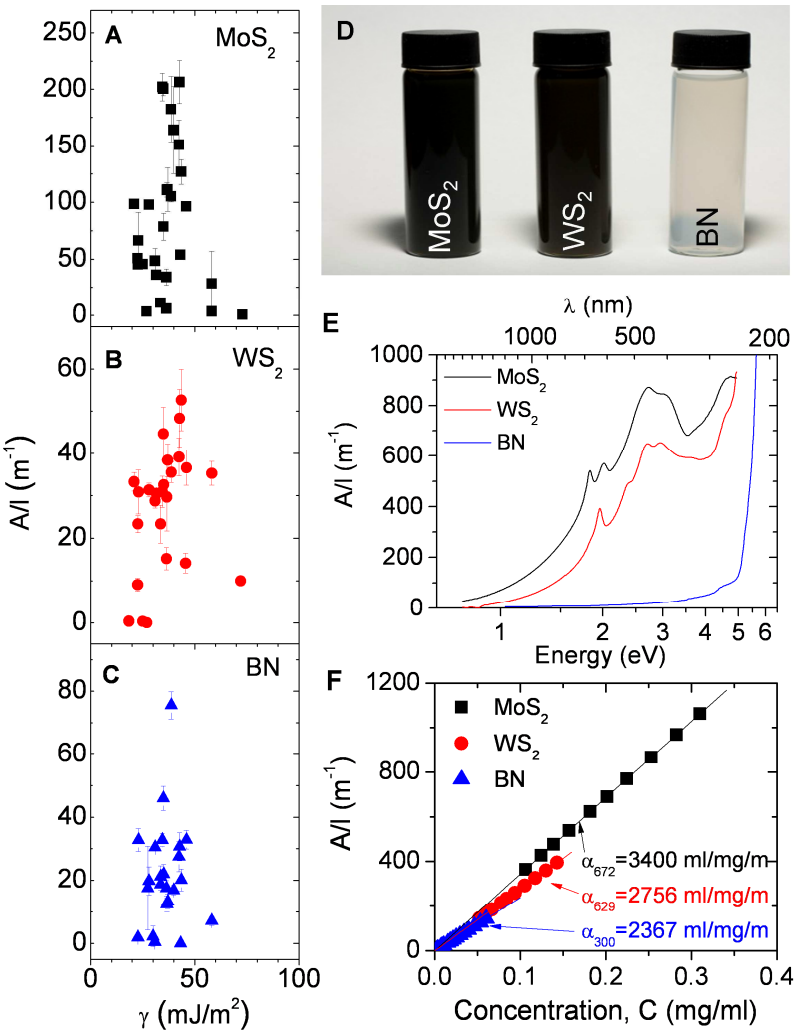

Fig. 1: Optical characterisation of nano-sheet dispersions. A), B) and C) Concentration remaining after centrifugation (plotted as A/l) for MoS_2, WS_2 and BN dispersed in a range of solvents, plotted versus solvent surface tension. D) Photographs of dispersions of MoS_2 (in NMP), WS_2 (in NMP) and BN (in IPA). E) Absorbance spectra of dispersions of MoS_2 (NMP, 0.16 mg/ml), WS_2 (NMP, 0.15 mg/ml) and BN (IPA, 0.002

mg/ml) F) Lambert–Beer plots for MoS_2 (NMP), WS_2 (NMP) and BN (IPA). The dispersions in D), E) and F) were prepared using optimised dispersion conditions (*25*).

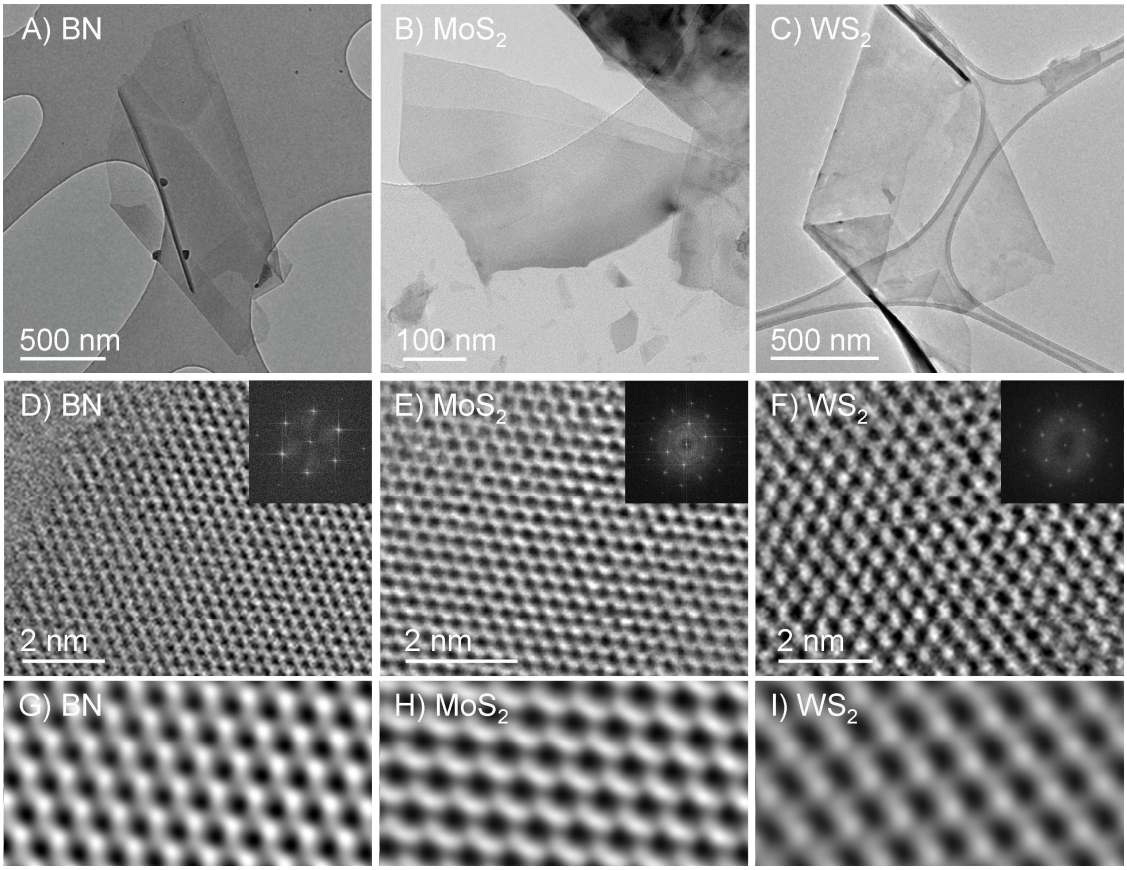

Fig. 2: TEM of nano-sheets. A), B) and C) Low resolution TEM images of flakes of BN, MoS_2 and WS_2 respectively. D), E) and F) High resolution TEM images of BN, MoS_2 and WS_2 monolayers. Inset: Fast Fourier transforms of the images. G), H) and I) Butterworth filtered images of sections of the images in D), E) and F).

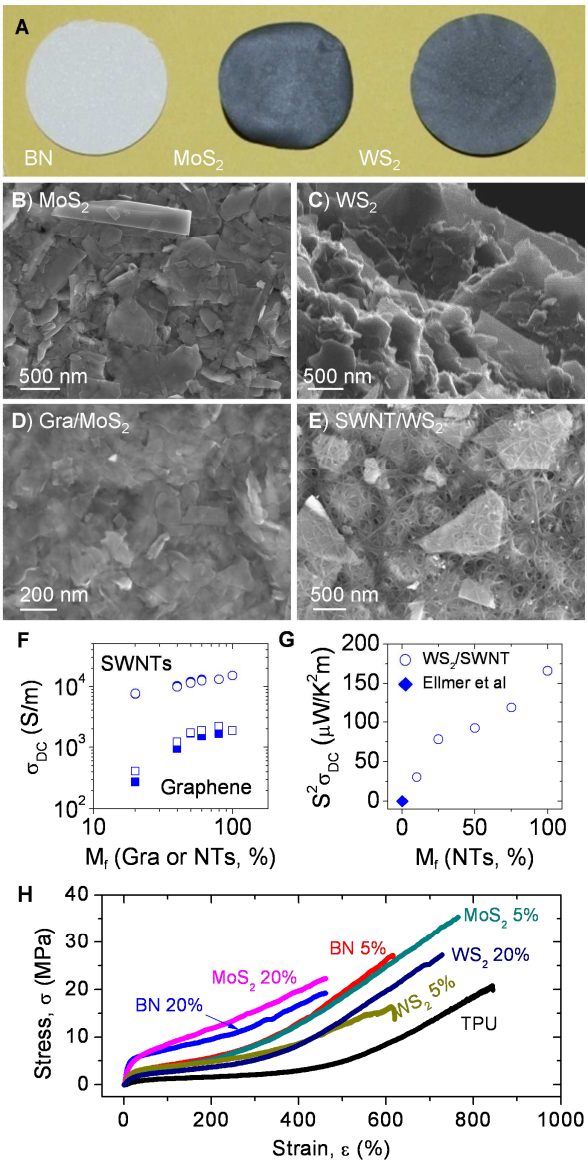

Fig. 3: Nano-sheet films, hybrids and composites. A) Photograph of free standing films of BN, MoS_2 and WS_2 (thickness ~50 µm). B) An SEM image of the surface of an MoS_2 film. C) He ion microscope image of the edge of a WS_2 film. D and E) SEM images of the surface of a graphene/MoS_2 hybrid film and a SWNT/ WS_2 hybrid film respectively. F) DC conductivity of thin (~200 nm) hybrid films prepared from mixtures of WS_2 or MoS_2 (open or closed symbols) and SWNTs or graphene (circles or squares). G) Product

of Seebeck coefficient squared and DC conductivity (the power factor) for thick (~50 μm) WS_2/SWNT hybrid films. While the WS_2 film proved too brittle to measure, Ellmer *et al.* measured $S^2\sigma$=0.22 μW/K^2m for a disordered WS_2 film. In F) and G), the x-axis is the mass fraction of SWNTs or graphene. H) Representative stress-strain curves for composites of polyurethane filled with each layered compound at loading levels of 5wt% and 20wt%.

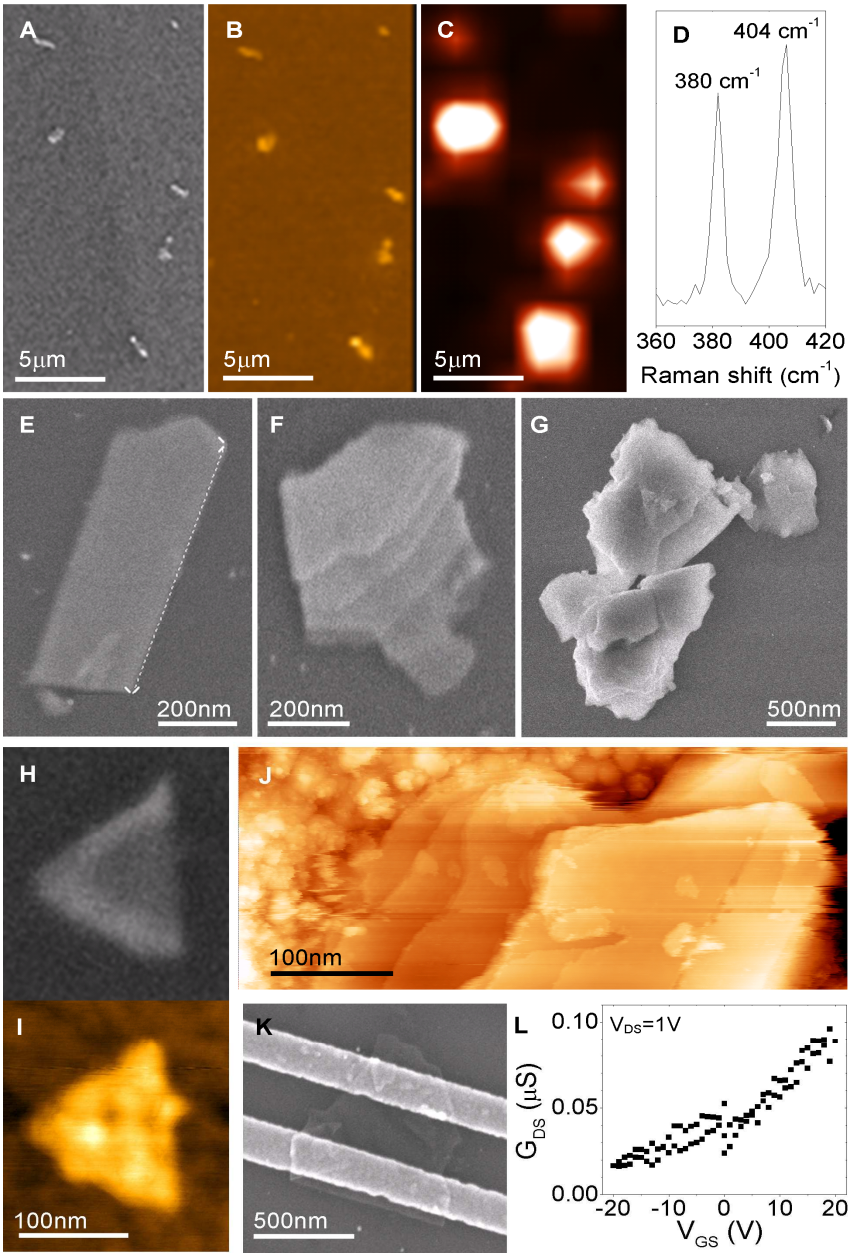

Fig. 4: Deposition of nano-sheets onto surfaces. A) and B) An SEM and an AFM image of MoS_2 flakes deposited on SiO_2 by spraying. C) A Raman map of the same region. D) Typical Raman spectrum of an individual flake. The Raman map plots the integral of the spectrum between 390 and 410 cm^{-1}. E), F) and G) A very thin flake, a multilayer and a

cluster of aggregated multilayers. The dashed line in E has been inserted to illustrate the straightness of the flake edge. H) and I) SEM and AFM images of an individual flake. J) An STM image of an individual flake. The flakes in I) and J) have heights of 5 and 10 nm respectively.(*25*) K) An SEM image of an MoS_2 flake on Si/SiO_2 with electrodes deposited on top. L) Source-drain conductance as a function of gate voltage for the flake shown in K).

References

1. S. K. Mishra, S. Satpathy, O. Jepsen, *Journal of Physics-Condensed Matter* **9**, 461 (1997).
2. E. A. Marseglia, *International Reviews in Physical Chemistry* **3**, 177 (1983).
3. J. A. Wilson, A. D. Yoffe, *Advances in Physics* **18**, 193 (1969).
4. F. R. Gamble, B. G. Silbernagel, *Journal of Chemical Physics* **63**, 2544 (1975).
5. F. Clerc *et al.*, *Journal of Physics-Condensed Matter* **19**, 17 (2007).
6. A. K. Geim, *Science* **324**, 1530 (2009).
7. B. Poudel *et al.*, *Science* **320**, 634 (2008).
8. A. Splendiani *et al.*, *Nano Letters* **10**, 1271 (2010).
9. K. S. Novoselov *et al.*, *Proceedings of the National Academy of Sciences of the United States of America* **102**, 10451 (2005).
10. A. Ayari, E. Cobas, O. Ogundadegbe, M. S. Fuhrer, *Journal of Applied Physics* **101**, (2007).
11. R. Ruoff, *Nature Nanotechnology* **3**, 10 (2008).
12. P. Joensen, R. F. Frindt, S. R. Morrison, *Materials Research Bulletin* **21**, 457 (1986).
13. C. Liu, O. Singh, P. Joensen, A. E. Curzon, R. F. Frindt, *Thin Solid Films* **113**, 165 (1984).
14. H. Matte *et al.*, *Angewandte Chemie-International Edition* **49**, 4059 (2010).
15. A. Nag *et al.*, *ACS Nano* **4**, 1539 (2010).
16. C. Y. Zhi, Y. Bando, C. C. Tang, H. Kuwahara, D. Golberg, *Advanced Materials* **21**, 2889 (2009).
17. Y. Hernandez *et al.*, *Nature Nanotechnology* **3**, 563 (2008).
18. S. D. Bergin *et al.*, *Advanced Materials* **20**, 1876 (2008).
19. S. D. Bergin *et al.*, *ACS Nano* **3**, 2340 (2009).
20. E. A. Ponomarev, M. NeumannSpallart, G. Hodes, C. LevyClement, *Thin Solid Films* **280**, 86 (1996).
21. J. P. Wilcoxon, P. P. Newcomer, G. A. Samara, *Journal of Applied Physics* **81**, 7934 (1997).
22. R. Bissessur, M. G. Kanatzidis, J. L. Schindler, C. R. Kannewurf, *Journal of the Chemical Society-Chemical Communications*, 1582 (1993).
23. G. L. Frey, K. J. Reynolds, R. H. Friend, H. Cohen, Y. Feldman, *Journal of the American Chemical Society* **125**, 5998 (2003).
24. R. A. Gordon, D. Yang, E. D. Crozier, D. T. Jiang, R. F. Frindt, *Physical Review B* **65**, (2002).
25. *See supporting material on Science Online.*
26. M. S. Dresselhaus *et al.*, *Advanced Materials* **19**, 1043 (2007).
27. K. Ellmer, C. Stock, K. Diesner, I. Sieber, *Journal of Crystal Growth* **182**, 389 (1997).
28. E. Benavente, M. A. S. Ana, G. González, *physica status solidi (b)* **241**, 2444 (2004).

29. R. F. Frindt, D. Yang, *Molecular Crystals and Liquid Crystals Science and Technology Section a-Molecular Crystals and Liquid Crystals* **311**, 367 (1998).
30. J. P. Lemmon, J. H. Wu, C. Oriakhi, M. M. Lerner, *Electrochimica Acta* **40**, 2245 (1995).
31. B. H. Xu, B. Z. Lin, D. Y. Sun, C. Ding, *Electrochimica Acta* **52**, 3028 (2007).
32. U. Khan, P. May, A. O'Neill, J. N. Coleman, *Carbon* **48**, 4035 (2010).
33. S. M. Liff, N. Kumar, G. H. McKinley, *Nature Materials* **6**, 76 (2007).
34. C. Lee *et al.*, *ACS Nano* **4**, 2695 (2010).
35. M. Osada, T. Sasaki, *Journal of Materials Chemistry* **19**, 2503 (2009).
36 The authors would like to acknowledge IRCSET (Embark Initiative), the European Research Council and Science Foundation Ireland (grant number 07/IN.7/I1772), for financial support. VN would like to acknowledge funding from the Marie Curie grant PIEF-GA-2008-220150 and the Royal Academy of Engineering/EPSRC and thank BegbrokeNano for their provision of research facilities.